Novel algorithms for efficiently accumulating, analysing and visualising full-waveform LiDAR in a volumetric representation with applications to forestry

submitted by

Milto Miltiadou

for the degree of Doctor of Engineering

of the

University of Bath

Centre for Digital Entertainment

and of the

Plymouth Marine Laboratory

NERC Airborne Research Facility

April 2017

Abstract

no more than 300 words

NOTES:

Blue colour: additions according to Neill's feedback,

Purple colour: addition/corrections according to Mike's comments

Red colour: notes

Gray colour: text that is going to be modified

To be added on top

Abstract

This study focuses on enhancing the visualisations and classifications of forested areas using coincident full-waveform (fw) LiDAR data and hyperspectral images. The ultimate aim is use both datasets to derive information about forests and show the results on a 3D virtual, interactive environment. Influenced by Persson et al (2005), voxelisation is an integral part of this research. The intensity profile of each full-waveform pulse is accumulated into a voxel array, building up a 3D density volume. The correlation between multiple pulses into a voxel representation produces a more accurate representation, which confers greater noise resistance and it further opens up possibilities of vertical interpretation of the data. The 3D density volume is then aligned with the hyperspectral images using a 2D grid similar to Warren et al (2014) and both datasets are used in visualisations and classifications.

Previous work in visualising fw LiDAR has used transparent objects and point clouds, while the output of this system is a coloured 3D-polygon representation, showing well-separated structures such as individual trees and greenhouses. The 3D density volume, generated from the fw LiDAR data, is polygonised using functional representation of object (FReps) and the marching cubes algorithm (Pasko and Savchenko, 1994) (Lorensen and Cline, 1987). Further, an optimisation algorithm is introduced that uses integral volumes (Crow, 1984) to speed up the process of polygonising the volume. This optimisation approach not only works on non-manifold object, but also a speed up of up to 51% was achieved. The polygon representation is also textured by projecting the hyperspectral images into the mesh. In addition, the output is suitable for direct rendering with commodity 3D-accelerated hardware, allowing smooth visualisation.

In future work, the effects of combining both hyperspectral imagery and fw LiDAR in classifications and visualisations are examined. At first, two pixel wise classifiers, a support vector machine and a Bayesian probabilistic model, will be used for testing the effects of the combination in generating tree coverage maps. Higher accuracy classification results are expected when metrics from both datasets are used together. Regarding the visualisations, the differences of applying surface reconstruction versus direct volumetric rendering will be discussed and an ordered tree structure with integral sums of the node values will be used for speeding up the ray-tracing of direct volumetric rendering and improving memory management of aforementioned optimisation algorithm with integral volumes. Further, deferred rendering is suggested for testing the visual human perception of projecting multiple bands of the hyperspectral images on the FW LiDAR

polygon representations. At the end of this project the combination of the datasets will be used along with the watershed algorithm for tree segmentation, which is useful for measuring the stem density of a forest and for tree species classifications.

from EDE:

Firstly, a new and fast way of aligning the FW LiDAR with Remotely Sensed Images has been developed in DASOS and by generating tree coverage maps it was shown that the combination of those datasets confers better remote survey results. This work was presented at the 36th ISRSE International Conference.

Secondly, automated detection of dead trees in native Australian forests has a significant role in protecting animals, which live in those trees and are close to extinction. DASOS allow the generation of 3D signatures characterising dead trees. A comparison between the discrete and FW LiDAR is performed to demonstrate the increased survey accuracy obtained when the FW LiDAR are used.

Finally, the last application is for improving visualisations for foresters. Foresters have a great knowledge about forests and can derive a wealth of information directly from visualisations of the remotely sensed data. This reduces the travelling time and cost of getting into the forests. This research optimises visualisations by using the new FW LiDAR representations and a speed of up to 51% has been achieved.

FW LiDAR has great potentials in forestry and this research has already started to have an impact in the FW LiDAR community by making those huge datasets easier to handle. DASOS is now used at Interpine Group Ltd, a world leading Forestry Company in New Zealand and it has been tested from a PhD student at Bournemouth University who looks into estimating bird distribution in the New Forest. In the future, it is expected that DASOS will be widely used in remote forest surveys (i.e. estimating the commercial value of a forest and detecting infected trees at early stages for treatment).

Acknowledgements

Above all, I would like to express my great gratitude to my industrial supervisors Dr. Michael Grant who had supported me continuously during my research and gave me the freedom to create a project of my own interest.

Then, I would like to thanks Dr. Matthew Brown, who helped me during my first years of my studies by giving me valuable and informative feedback. He was always there to keep me working on the right track.

Equally important is my current supervisor Dr. Neil D.F. Campbell and he is not to be missed from the acknowledgements.

Furthermore, special thanks are given to Dr. Mark Warren, Dr. Darren Cosker, MSc Susana Gonzalez Aracil and Dr. Ross Hill who occasionally advised me during my studies.

It further worth giving credits to my data providers, the Natural Environment Research Council's Airborne Research Facility (NERC ARF) and Interpine Group Ltd.

Last but not least, I am extremely grateful to my funding organisations, the Centre for Digital Entertainement and Plymouth Marine Laboratory, who supported financially and consequently made this research possible.

Abbreviations and Glossary

AGC	Automatic Gain Controller
ALS	Airborne Laser Scanning
APL	Airborne Processing Library
ARF	Airborne Research Facility
CG	Computer Graphics
CHM	Canopy Height Model
CUDA	parallel computing platform available on nvidia graphic cards
DASOS	($\delta\alpha\sigma o\varsigma$=forest in Greek), the open source software implemented for managing FW LiDAR data
DBH	Diameter at Breast Height
DEM	Digital Elevation Model
DTM	Digital Terrain Model (DTM)
FN	False Negative
FP	False Positive
FW	Full-Waveform
GB	Gigabyte
K-NN	K-Nearest Neighbour
LiDAR	Light Detection And Ranging
MRI	Magnetic Resonance Imaging
NASA	National Aeronautics and Space Administration
NDVI	Normalised Difference Vegetation Index
NERC	Natural Environment Research Council
NIR	Near-Infrared Region of the electromagnetic spectrum
QGIS	Quantum Geographic Information System
SIMD	Single Instruction, Multiple Data
TB	Terabyte
TP	True Positive
TN	True Negative
VIS	VIsual Spectrum
VLR	Variable Length Records
WPDF	Waveform Packet Descriptor Format
UK	United Kingdom

Publications

DASOS-User Guide, M. Miltiadou, N.D.F Campbell, M. Brown, S.C. Aracil, M.A. Warren, D. Clewley, D.Cosker, and M. Grant, Full-waveform LiDAR workshop at Interpine Group Ltd, Rotorua NZ, 2016
Improving and Optimising Visualisations of full-waveform LiDAR data, M. Miltiadou, M. Brown, N.D.F Campbell, D. Cosker, M. Grant, *EuroGraphics UK, Computer Graphics & Visual Computing*, 2016
University of Bath **Alignment of Hyperspectral Imagery and Full-Waveform LiDAR data for visualisation and classification purposes**, M. Miltiadou, M. A. Warren, M. Grant, and M. Brown, *The International Archives of Photogrammetry, Remote Sensing and Spatial Information Sciences*, vol. 40, no. 7, p. 1257, 2015.
Reconstruction of a 3D Polygon Representation from Full-Wavefrom LiDAR data, M. Miltiadou, M. Grant, M. Brown, M. Warren, and E. Carolan,*RSPSoc Annual Conference, New Sensors for a Changing World*, 2014.

Awards

EDE and Ravenscroft Prize - Finalist: Selected as one of the five finalists for this is a prestigious prize that recognises the work of best postgraduate researchers.
Student Poster Competition at Silvilaser.

Conference Presentations

Remote Sensing Cyprus (RSCy) Conference, 2017 , Paphos, Cyprus - Oral Presentation
ForestSAT Conference,2016 , Santiago, Chile - Oral Presentation
Computer Graphics & Visual Computing (CGVC),2016, Bournemouth, United Kingdom - Poster Presentation
Silvilaser, 2015, La Grant Motte, France - Oral Presentation
International Symposium of Remote Sensing of the Environment (ISRSE), 2015, Berlin, German - Oral Presentation
Remote Sensing and Photogrammetry Society (RSPSoc) Conference, New Sensors for a Changing world , 2014, Aberystwyth, United Kingdom - Oral Presentation

Workshops

Full day workshop about FW LiDAR and DASOS at *Interpine Ltd Group*, 2016, Rotorua, New Zealand

Demonstration of DASOS_v2 at the practical LiDAR session at *the NERC ARF annual workshop*, 2017, Plymouth, United Kingdom

Contents

List of Figures

Chapter 1

Introduction

1.1 Forest Monitoring: Importance and Applications

1.2 Background Information about Remote Sensing and Airborne Laser Scanning Systems

Chapter 2

Acquire Data

Chapter 3

Overview of Thesis

Chapter 4

The open source software DASOS and the Voxelisation Approach

Chapter 5

Surface Reconstruction from Voxelised FW LiDAR Data

Chapter 6

Optimisation Attempts for the Surface Reconstruction

Chapter 7

Alignment with Hyperspectral Imagery

Chapter 8

Detection of Dead Standing Eucalyptus For Managing Biodiversity in Native Australian Forest

8.1 Introduction

8.1.1 The Importance of Dead Wood

The value of dead trees from a biodiversity management perspective is large. Once a tree dies, its contribution to our ecosystem continues. The woody structure remains for centuries and it contributes to forest regeneration while providing resources for numerous surrounding organisms [71]. As an indication, more than 4000 species inhabit dead wood in Finland [72], where an estimate of 1000 species has been extinct [73]. These species do not only include animals and birds but also organisms, like fungi. Fungi contributes to wood decaying, formation of hollows and biodiversity, which is an important factor for a resilient ecosystem [74]. Observing the changes of fungal diversity on decaying wood has an increased interest in science [75] [76] [77] in order to ensure the continuous existence of decaying wood in forests.

In Australia, tree hollows play a significant role in managing biodiversity. Nearly all arboreal mammals rely on hollows with the exception of the Koala and perhaps Ringtail Possums that preferentially make a stick nest, but they use hollows as well. Additionally, a large number of Australian bird species rely on hollows for shelters [5]. Nevertheless, Australia has no real hollow creators unlike the northern hemisphere (e.g. Woodpeckers), and therefore it relies predominantly on natural processes of limb breakage, insect and fungal attack when access points are provided through damage caused by wind, storms and fire.

This kind of hollows take hundreds of years to form and because of that it is more likely to exist on dead trees. In Australia, studies predict shortage of hollows for colonisation in the near future [3] [4]. Therefore automated detection of them plays a significant role in protecting those animals. As an indicator of the importance of hollows in managing biodiversity, a list of a few of the species that rely on hollows was provided by the Forestry Corporation of NSW. Those species are shown at Figure 8-1. According to the Department of the Environment of Australian Government and the Government of Western Australia, six of them are protected, threatened or close to extinct [78] [79]. Figure 8-1 shows the species from the provided list and the six protected species have a red border and their names are bold in the description.

For the aforementioned reasons, monitoring dead trees is essential for having a resilient ecosystem. Nevertheless, the distribution of dead trees significantly varies making detection of them difficult [80]. Remote sensing approaches has been introduce to automate the process of monitoring forest and further increase the spatial resolution of the monitored area. The following section gives an overview of the related work undertaken in Remote Sensing.

8.1.2 Related Work

Remote Sensing was introduced for automatically detecting dead trees, because field-work is time consuming considering their variance spread and the size of the relevant forests. From a classification perceptive, the task of identifying dead standing and dead fallen trees is different. Fallen trees are identified by detecting segments or line-like features on the terrain surface using LiDAR data [81] [82]. Regarding standing dead trees, their shape (reduced number of leaves or broken branches) [83] and light reflectance (less green light illuminated) [84] are important factors for identifying them.

Previous work on dead standing trees detection performs single tree crown delineation before health assessment [83] [85]. Tree-crown delineation is usually done by detecting local maxima from the canopy height model (CHM) and then segmenting trees with watershed algorithm [86]. Improvements has been achieved by introducing markers controlled watershed [87] and structural elements of tree crowns with different sizes [88]. Additionally, Popescu and Zhao analyse the vertical distribution of the LiDAR points in conjunction with the local maximum filtering of CHM [89].

In the case of Eucalyptus, single tree detection is a challenge on its own, due to their irregular structure and multiple trunk splits. In other words, each tree trunks splits

Figure 8-1: A number of species that rely on tree hollows of which the red ones / bold ones are close to extinction: Kookaburra, Sulphur Crested Cockatoo, **Corella**, Crimson Rosella, Eastern Rosella, Galah, Rainbow Lorikeet, Musk Lorikeet, Little Lorikeet , Red-winged Parrot, **Superb Parrot**, Cockatiel, Australian Ringneck (Parrot), Red-rumped Parrot, Powerful Owl, Sooty Ow, Barking Owl, **Masked Owl**, **Barn Owl**, White-throated Treecreeper, Hollow Owl, **Brush-tailed Possum** (mammal) [1]

[1]The images of the birds were taken from the following links (Retrieved on the 27th of April 2016): Kookaburra: `<http://tenrandomfacts.com/blue-winged-kookaburra/>`, Sulphur Crested Cockatoo: `<http://aussiegal7.deviantart.com/art/Sulphur-Crested-Cockatoo-08-153341893>`, Corella: `<http://www.theparrotplace.co.nz/all-about-parrots/long-billed-corella/`, Superb Parrot: `<http://www.davidkphotography.com/?showimage=637>`, Crimson Rosella: `<http://25.media.tumblr.com/tumblr_m3mo89c40r1r4t9h1o1_1280.jpg>`, Eastern Rosella: `<http://2.bp.blogspot.com/-pYxw51WjSOY/UB-LEFgd2KI/AAAAAAAAAWg/9z60PUWE6TE/s1600/_GJS6601-as-Smart-Object-1.jpg>`, Rainbow Lorikeet: `<https://www.reddit.com/r/pics/comments/328fvc/a_rainbow_lorikeet_found_in_coastal_regions/>`, Musk Lorikeet: `<http://www.rymich.com/girraween/photos/animals/birds/medium/glossopsitta_concinna/glossopsitta_concinna_001.jpg>`, Little Lorikeet: `<http://www.pbase.com/sjmurray/psittacidae>`, Red-winged Parrot: `<https://www.pinterest.com/pin/395894623469889727/>`, Cockatiel: `<http://up.parsipet.ir/uploads/Cockatiels-for-sale.jpg>`, Australian Ringneck (Parrot): `<http://ontheroadmagazine.com.au/wp-content/uploads/2015/09/Twenty-eight-parrot-2-min.jpg>`, Red-rumped Parrot: `<http://parrotfacts.net/wp-content/uploads/Red-Rumped-Parrot-on-a-tree.jpg>`, Powerful Owl: `<http://farm1.staticflickr.com/219/495796536_f78dac04c1.jpg>`, Sooty Owl: `<ttp://www.mariewinn.com/marieblog/uploaded_images/screech2-738532.jpg`, Barking Owl: `<http://www.pcpimages.com/Nature-and-Wildlife/Birds/i-7JKSTp5/1/L/owl%20%281%20of%201%29-L.jpg>`, Masked Owl: `<http://www.survival.org.au/images/birds/masked_owl_2_600.jpg>`, Galah: `https://www.pinterest.com/pin/537546905498955709/>`, White-throated Treecreeper: `<https://geoffpark.files.wordpress.com/2011/09/female-white-throated-treecreeper.jpg>`,

create a local maximum leading into over-segmentation when tree crowns are detected by local maxima filtering. Shendryk published a eucalyptus delineation algorithm that starts segmentation from bottom to top. In this paper, the trunks point cloud is separated from the leaves and individual trunks are identified before proceeding to crown segmentation [90]. Nevertheless, for that project only 17 flightlines of LiDAR data were collected. The density resolution starts from 12 points/m^2 and goes up to 36 points/m^2 around forested areas. For small research projects capturing this high resolution is acceptable, but for commercial use and larger areas, the density of data collected is above the optimal resolution for a cost effective versus quality acquisition [91]. The project of this thesis is much larger. The resolution of our acquired LiDAR data has an average of four pulses per square meter,which is considered an optimal resolution in relation to the cost. But because of the tree height (up to $43m$ according to the fieldwork), a small amount of pulse intensity reached the trunks and the recordered waveform do not include enough information for individual trunk detection. An example of this project's discrete LiDAR data is shown in Figure 8-2 and the missing information about the trunks is depicted.

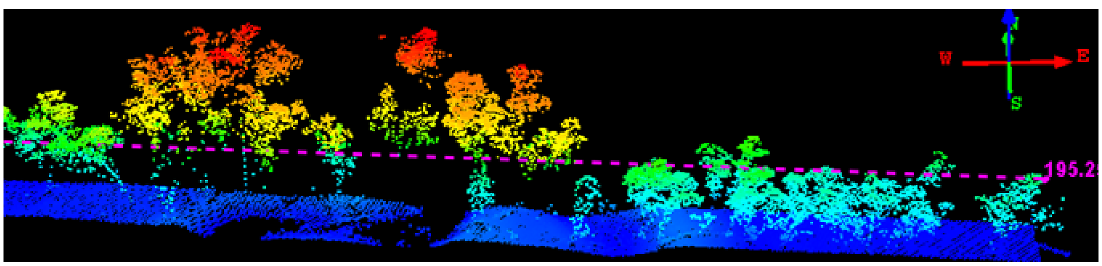

Figure 8-2: LiDAR point cloud showing that there are very limited points reflected from tree trunks.

***Note read again to make sure it matches OK

The acquired data are full-waveform LiDAR data. Traditional ways of interpreting FW LiDAR data, suggests extraction of a denser points cloud using Gaussian decomposition [29] [30]. Nevertheless, in this project we uses the open source software DASOS. DASOS was influenced by Persson et al [26], who used voxelisation to visualise the waveforms . But, it does not only uses voxelisation for visualisations but also for extracting metrics useful in classification. It further normalises the intensities so that equal pulse length exists inside each voxel, making intensities more meaningful. It is further seems that the literature is moving towards voxelisation with promising results obtained at recent publication on tree species classification [33].

Here, it is introduced an approach for quick dead tree detection derived from the

Hollow Owl: <http://www.mariewinn.com/marieblog/uploaded_images/screech2-738532.jpg>

boost cascade approach [92] but extended into 3D. This approach further contains similarities of the 3D tree shape signatures proposed by Dong, 2009, for distinguishing Oaks from Douglas fir tree crowns [93].

8.2 Materials

8.2.1 Study Area

The study area (Figure 8-3) is a native River Red Gum (Eucalyptus camaldulensis) forest of size $542km^2$ in south-eastern Australia. The regeneration of the eucalyptus is extremely dependant in floods and therefore, their distribution in respect to density, health and age is highly variance [94]. Additionally, the height of Eucalyptus camaldulensis reaches up to $30-40m$ and their structural complexity is high with multiple trunk splits [95]. The size and structure of the forest, with a human as reference, is depicted in Figure 8-4, while examples of the variance shape of dead trees is shown in Figure 8-5.

8.2.2 Acquired full-waveform LiDAR data

Multiple-echo, full-waveform (FW) LiDAR data are supplied by RPS Australia East Pty Ltd. The data were acquired from 900m above ground level, using the Trimble AX60 Airborne LiDAR sensor, which was released in October 2013 [96]. The wavelength of the emitted laser was 1062nm, the maximum scan angle was 60 degrees, and the pulse rate was 400kHz. The acquisition was held from the 6th of March till the 31st of March 2015. The collected LiDAR were delivered into 206 flightlines, of which 13 are cross runs used for geometric correction. There is also a 30% of swath overlap. The point spacing along and across the track is 0.48m and the average point spacing is 4.3 points per square meter. Figure 8-6 shows an example of a dead tree in respect to the acquired discrete LiDAR point cloud. Detailed information about FW LiDAR related concepts are given in section 2.

8.2.3 Field Data

The field data were collected in July 2015 during the winter season of Australia and they include tree and canopy related measurements on circular plots. There are 33 plots with radius 35.68m and area 0.4ha allocated randomly inside the study area. On these plots, a total of 2386 trees were individually measured. Tree measurements include the geo-location, the trunk diameter at the standard height of 1.3m (breast heigh), height, species and health conditions (i.e. dead or alive). The geo-location of each tree is defined

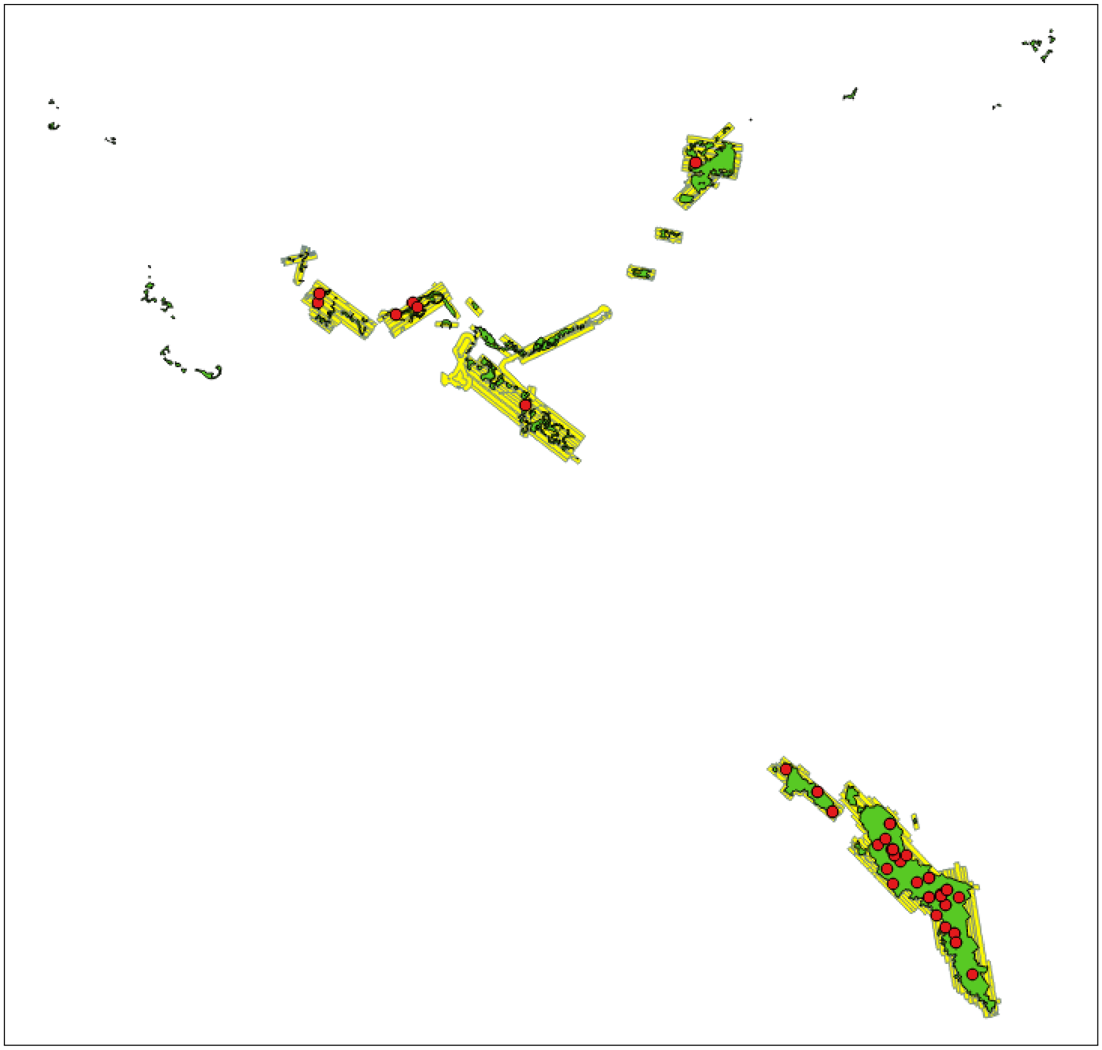

Figure 8-3: The study area is depicted by green ($542km^2$), the yellow strips are the LiDAR flightlines and the red dots are the position of the field plots.**Note: this image many need to be removed due to confidentiality of the company. I will talk with them and hopefully it will be ok.

by the magnetic bearing from the centroid of the plot in degrees (range $[1, 360]$) and the distance from the centroid in meters. The northing and easting coordinates of the geo-location of each tree were calculated in post-processing. Here is worth mentioning that a single tree may be recorded as multiple trees if there is a trunk split bellow the breast height of 1.3m. Furthermore, 91.59% are River Red Gum and the rest are Black Box (Eucalyptus largiflorens) and Wattle group (Acacia spp.).

Inside the field data, there are 260 dead trees recorded. Nevertheless, not all of those trees are considered useful for biodiversity. Dead trees with big Diameter at

Figure 8-4: Structure of Red Gum Forest in south-eastern Australia.

Figure 8-5: Example of dead trees indicating their variance in shape.

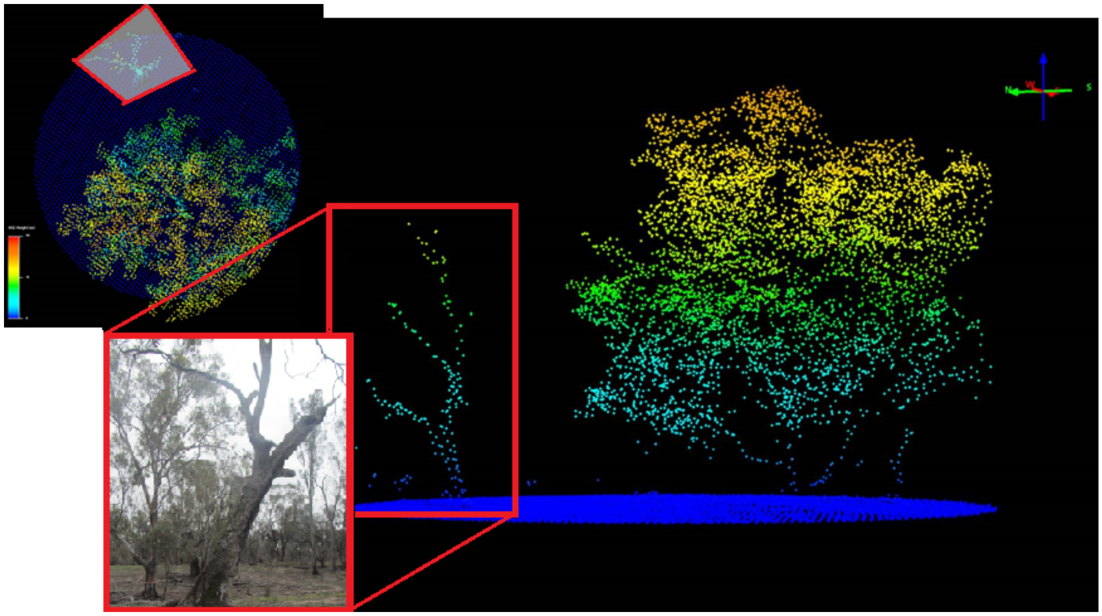

Figure 8-6: Example of a dead tree in relation to the discrete LiDAR point cloud.

Breast Height (DBH) are more likely to contain hollows. Additionally, trees with DBH smaller than the footprint spacing of the LiDAR data are not identifiable from the FW LiDAR data. Table **??** shows the number of dead and alive trees in respect to their DBH.

DBH (cm)	Dead Trees	Alive Trees
>2000	0	1
1000-2000	7	21
600-1000	8	146
400-600	26	290
300-400	32	286
200-300	50	462
100-200	125	904
<100	11	16
Total	260	2126

Table 8.1: Number of trees according to their DBH

Please note that the aforementioned field data were provided by Forestry Corporation of NSW, Wauchope, Australia and Interpine Ltd Group, New Zealand. For this thesis, a case study for collecting field data was conducted in New Forest, UK. This helped to better understand classification challenges in forestry applications. More information about this study is provided in Appendix B.

8.3 Classification Challenges

This section focuses on the challenges faced while working on the detection of dead standing eucalyptuses. Table 8.2 underlines these challenges, categorised into three groups: the nature of the study area, the acquired data and the field data. All these challenges influence the quality of the classifier and the accuracy of the results.

Study Area	**Acquired Data**	**Field Data**
• The study area is a native eucalyptus forest. Native forests contain trees of different ages and heights. The height of a dead tree could be within the range of [1.5,40] meters. • There is a high variance in the density of the forest. Sometimes the testing/training priors of the small dead trees may contain information from either nearby alive trees or ground. • A tree may have dead branches but still be alive. • Eucalyptus trees have irregular shapes and multiple trunk splits making tree delineation to require very dense acquired data.	• The pulse density of the acquired data does not allow bottom to top tree delineation. Crown detection from DEM (top) leads to over-segmentation due to the multiple trunk-splits. We, therefore, investigate the performance of object detection algorithms that do not require tree delineation. • An important factor of identifying dead trees is the light reflectance, but for this project this kind of data (i.e. coloured imagery) was not acquired. Therefore, the classifier is only trained on tree shapes. But the shape of the tree is not an independent factor of identifying dead trees, since a tree may not have leaves but still be alive.	• If a tree has a trunk split below the 1.3m height, then it is recorded as multiple trees within the field data. This results into an inconsistency of the "one tree" concept. • They contain small trees, which are non detectable from the acquired data. • The accuracy of the geo-spatial positions is unknown. Even though it is claimed to be within centimetres, there are trees clearing appearing on the ground, once visualised on top of the DEM. An example: 

Table 8.2: The Classification challenges of automated detection of dead eucalyptuses

8.4 Methods and Algorithms

This section provides an explanation of the algorithms implemented. An overview of the work flow is given here:

1. Subtraction of the Digital Terrain Model (DTM) from the FW LiDAR data
2. Generation of training feature vectors characterising dead and alive trees, as well as testing samples of unknown population
3. Identification of the most important relevant features using random forest
4. Generation of a probabilistic field using a weighted k-nearest neighbour (KNN) algorithm.
5. Filtering
6. Height histogram and ground pixels removal
7. Thresholding dead pixels from alive, filtering, applying a seed growth algorithm for grouping nearby pixels and assignment of dead trees position.

8.4.1 Subtract DTM from FW LiDAR

A feature was implemented in DASOS for subracting pre-calculated Digital Terrain Model (DTM) saved into .bil files. Generating a DTM is beyond the scope of this research and the DTM files used were provided by Interpine Ltd Group. The provided DTM files were generated using the Quick Terrain Modeller from discrete LiDAR using the parameters shown in Figure 8-7.

The subtraction of the DTM is done during the voxelisation (Section 4). The terrain height is subtracted from the position of the sample before it is inserted into the volume. Please note that each terrain value is not subtracted from the origin of its pulse but from the position of each sample since the terrain value at the origin and the terrain value at the position of a sample may differ.

Figure 8-8 shows an example of a DEM generated before and after the subtraction using DASOS.

8.4.2 Generating feature vectors using DASOS

The feature vectors is a new feature of DASOS (version 2), which was released on the 20th January 2017 [97]. The dead tree detection is its first application. This feature is useful for characterising object inside the 3D space (e.g. trees). For each column

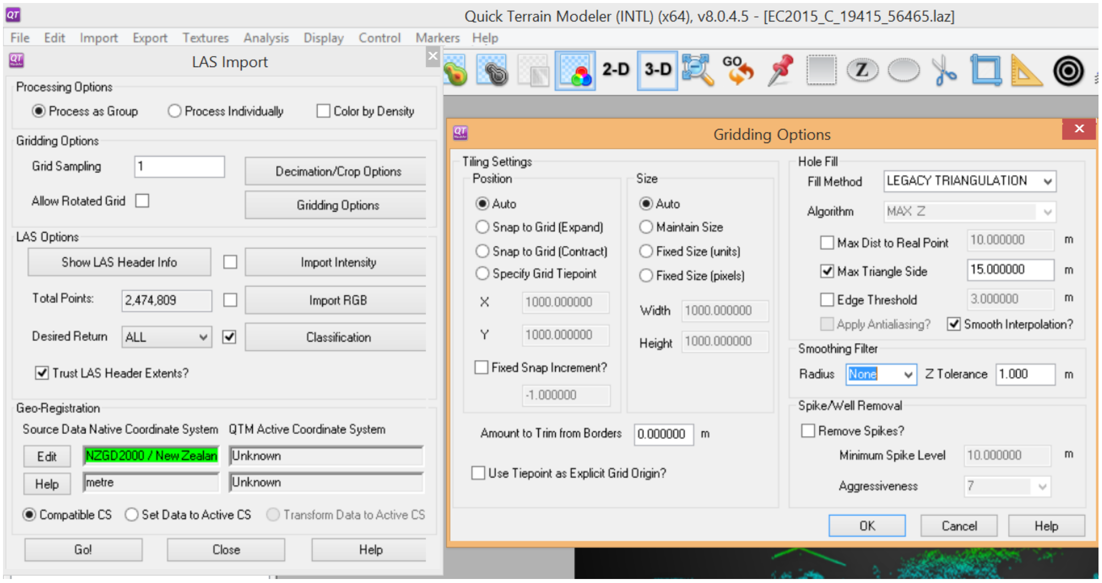

Figure 8-7: Parameters used in Quick Terrain Modeller to obtain the DTM used here.

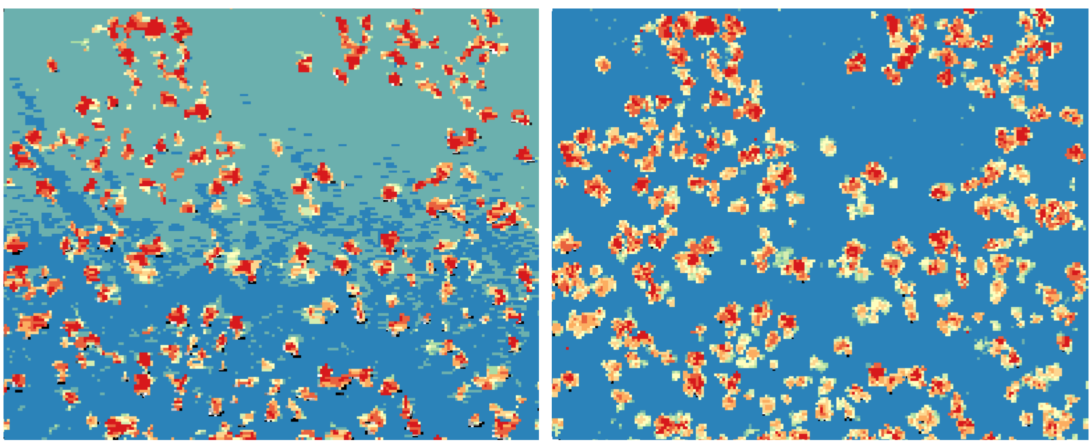

(a) The DEM before subtracting the DTM (b) The DEM after subtracting the DTM

Figure 8-8: The difference of the DEM before and after subtracting the terrain height. The red indicates big height, while the darker the blue is the lower the DEM is.

of interest within the voxelised FW LiDAR data, information around its local area are exported as feature vector. Multiple feature vectors are listed within .csv files for easy manipulation into software packages specialised in statistical analysis like R and matlab. There are two types of exported information from these local areas: processed and raw. If the processed option is chosen, then information like the distribution of non-empty voxels and the standard deviation of heights are listed. A sample of the exported processed information along with explanations is given in Table 8.3, while the entire list is provided within the Appendix A. If the exported parameters are raw, then the corresponding intensity values of the local area's voxels are exported. Additionally, there are two available shapes of the local area from where the features are extracted (the cuboid and the cylinder). The size of shape is also user defined. Here, the aforementioned feature of DASOS is used for generating feature vectors used as a likelihood in the classifier.

Explanation of some features of DASOS's 3D priors that proved to be useful for building the classifier		
No	**Label**	**Description**
1	Height_Middle_Column	The height of the middle column of the prior
	Height_Mean	The Mean height of all the columns included in the template
	Height_Median	The Median height of all the columns included in the template
1	Height_Std	The Standard Deviation of the heights of the columns included in the template
2	Top_Patch_Len_Std	The Standard Deviation of all the top patches
3	Dis_Std	The Standard Deviation of the distances between the central voxel and every voxel that contains an intensity above the isolevel
4	Per_Int_Above_Iso	Percentage of voxels that contain an intensity above the isolevel
5	Top_Patch_Len_Mean	The Mean length of all the top patches
	Top_Patch_Len_Median	The Median length of all the top patches
7	Dis_Mean	Mean distance from the central voxel to every voxel that contain san intensity above the isolevel
8	Dis_Median	Median distance from the central voxel to every voxel that contains an intensity above the isolevel
9	Sum_Int_Diff_Z	The Mirror Summed Difference of the intensities using the middle column in the z-axis as the axis of symmetry
10	Sum_Int_Diff_X	The Mirror Summed Difference of the intensities using the middle column in the x-axis as the axis of symmetry

Table 8.3: Explanation of some features of DASOS's 3D priors that proved to be useful for building the classifier. All the features are explained in Appendix A

Within the field data, some plots exist on two flightlines due to the overlapping of the flights. Overlaps happen at the edges of the flightlines and their scan angle significantly varies. For that reason, each unique set of field plots and corresponding flightlines is considered as a test/training plot. This results into 50 plots. These plots were randomly divided into 5 equal training datasets. Another dataset was also created by merging the first, second and third dataset in order to check whether the increased training data improves the classification accuracy.

The feature vectors generated for each field plot are divided into two categories (processed and raw intensities) and two sub-categories (cylinder and cuboid shape), resulting into four types of feature vectors per plot. For each type, three .csv files are generated. The first one contains the feature vectors characterising the dead trees, the second one contains the feature vectors of the alive trees and the third one contains one feature vector for each column of the voxelised space. The first two are used for training the classifier and the last one for testing. The dimensions of their shapes were chosen to be a bit smaller than the estimated average size of the dead trees to reduce the size of the irrelevant information contained within the priors. Figure 8-9 depicts the divisions of the datasets and the information about the feature vectors generated.

8.4.3 Random Forest

Random Forest is able to identify the importance of predicting variables. At first, it generates multiple regression trees by randomly sampling the data at its nodes and choosing the best predicting variables for each sampled data. The variable importance is then defined according to influence it has to the classification once this variable is modified and the rest remain unchanged [98]. In this project, the R package is used for finding the most relevant feature of the 3D priors (Section 8.4.2 in identifying dead trees.

At this point, it worth highlighting that Random Forest failed to find relation between the 3D priors with the "Raw Intensities" due to the irregular shapes of Eucalyptus trees and the variant scan angle of each field plot. Nevertheless, "Raw Intensities" may be useful for other classification, e.g. pine trees in commercial forest, where their shape variance is smaller.

Regarding the "Processed Intensities", Figure 8-10 shows a list with the variable importance according to Random Forest and Table 8.3 gives the explanation of each important variable identified. The most important one is the standard deviation of height. This is reasonable since the canopy of dead trees has bigger height variance in comparison to alive trees whose canopy is leafy. Please note that in Figure 8-10 the union of all datasets is used and that the significant features slightly vary depending on each sub dataset used.

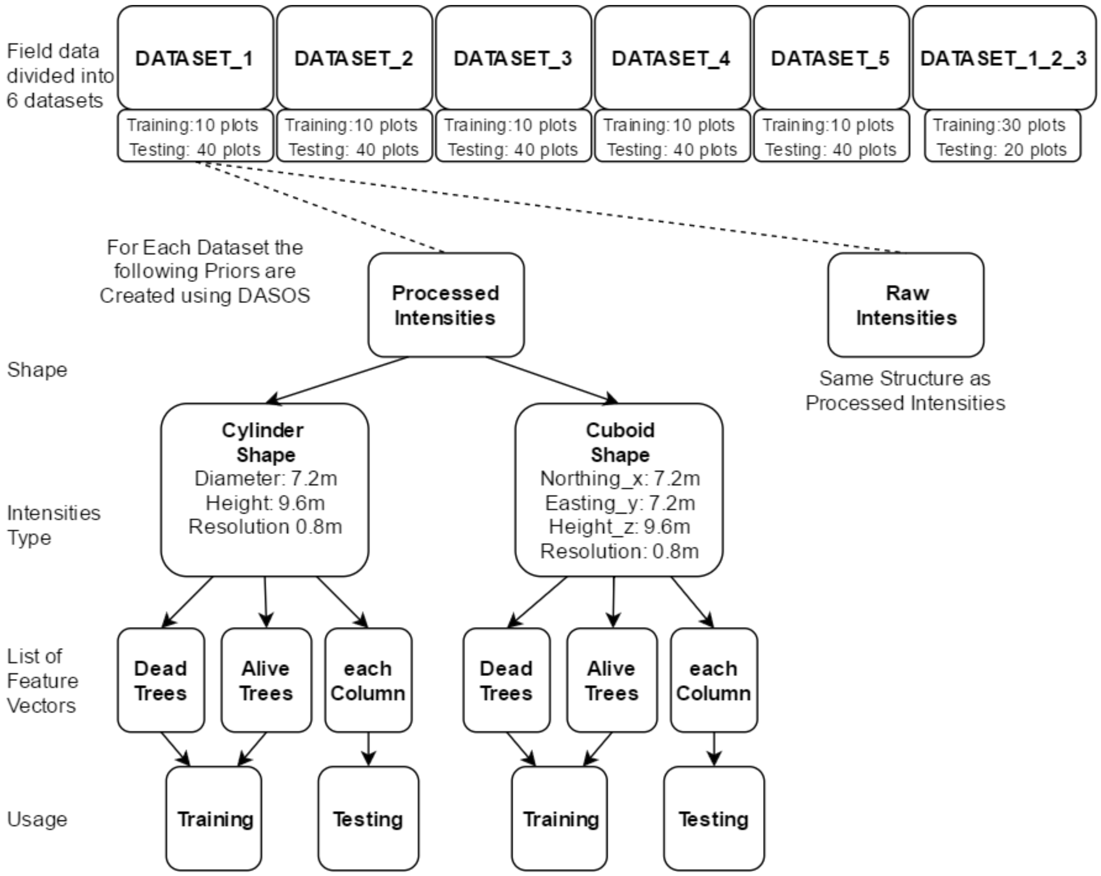

Figure 8-9: This figure shows what feature vectors were created for testing and how they are divided for cross validation.

8.4.4 **New : Probabilistic Field derived from Weighted K-Nearest Neighbours Algorithm

Once the ten most significant variables are identified using the Random Forest, the $k-$nearest neighbour algorithm is applied to generate a probabilistic field. As mentioned in Section 8.4.2, from DASOS we export training feature vectors of dead and alive trees. There are positive training feature vectors from dead trees and negative feature vectors for alive trees. To reduce bias, the number of dead and alive trees used are the same for each test case.

Let's assume that T is a training dataset with n feature vectors:

$$T : \big(x_n, f(x_n)\big), n = 1 \dots N. \tag{8.1}$$

The outputs of function $f(x_n) \in \{0, 1\}$. The value 0 indicates that the feature vector x_n was derived from an alive tree and the value 1 from a dead tree. For example

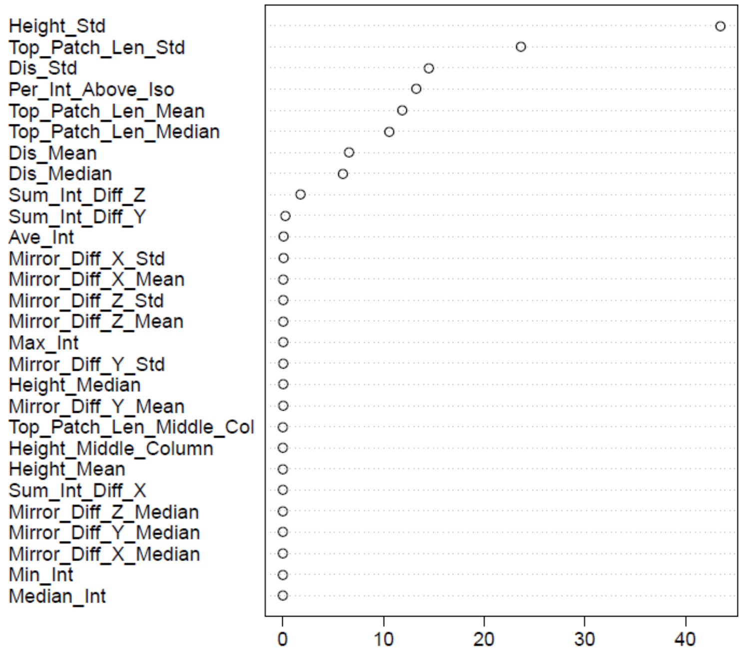

Figure 8-10: Importance of variables, identified using Random Forest.

the dataset T has this form:

$$T : (\boldsymbol{t_1}, 1), (\boldsymbol{t_2}, 0), (\boldsymbol{t_3}, 0), (\boldsymbol{t_4}, 1).......(\boldsymbol{t_n}, 1) \tag{8.2}$$

Every feature vector $\boldsymbol{t_q} \in T$ contains the 10 most important features exported from DASOS, as they were identified from the Random Forest algorithm ($\boldsymbol{t} = \{t_1, t_2, \ldots, t_{10}\}$). Additionally, every feature is associated with a weight value according to its importance ($\boldsymbol{w} = \{w_1, w_2, \ldots, w_{10}\}$). Additionally:

$$\boldsymbol{t_q} \begin{cases} t_1 \\ t_2 \\ \ldots \\ t_{10} \end{cases} \in R^d \qquad\qquad \boldsymbol{w} \begin{cases} w_1 \\ w_2 \\ \ldots \\ w_{10} \end{cases} \in R^d \tag{8.3}$$

Let's define a data vector $\boldsymbol{x} = (x_1, \ldots, x_10)$ of an unknown population. How do we calculate the probability of vector $\boldsymbol{x}$ to belong to the dead trees population? At first, the weighted Euclidean distance from $\boldsymbol{x}$ to every $\boldsymbol{t_q} \in T$ is calculated as follow:

$$d(\boldsymbol{t_q}, \boldsymbol{x}) = \sqrt{\sum_{i=1}^{10} \Big(w_i \times (t_{qi} - x_i)^2\Big)} \tag{8.4}$$

Then the $k-$nearest training samples are selected. In this project $k = 7$ was considered reasonable in respect to the size of each testing case. In the future, testing different values of k could evaluate how well the algorithm performs in relation to k. The nearest 7 indices of the training samples are selected as follow:

$$q = \operatorname*{argmin}_{\boldsymbol{t} \in T} d(\boldsymbol{t}, \boldsymbol{x}) \tag{8.5}$$

The dataset $V = \{\boldsymbol{v_1}, \boldsymbol{v_2}, \ldots, \boldsymbol{v_7}\}$ is a subset of the training samples T and contains the k-nearest indices to $\boldsymbol{x}$. The dataset V may contains samples derived from either dead trees, alive trees or both.

For each $\boldsymbol{v_i} \in V$ a weight $\boldsymbol{u_i}$ is calculated:

$$u_i = \frac{1}{d(\boldsymbol{t_i}, \boldsymbol{i})} \tag{8.6}$$

By the end, the probability of a dead tree is given by the following equation:

$$P(\text{dead}) = \frac{\sum_{i=1}^{k} \Big(u_i \times \delta\big(1, f(\boldsymbol{v_i})\big)\Big)}{\sum_{i=1}^{k} \Big(u_i \times \delta\big(1, f(\boldsymbol{v_i})\big)\Big) + \sum_{i=1}^{k} \Big(u_i \times \delta\big(0, f(\boldsymbol{v_i})\big)\Big)} \tag{8.7}$$

where the function $\delta(a, b)$ returns 1 if a is equal to b and 0 otherwise.

For each column of the voxelised FW LiDAR data, a testing data vector $\boldsymbol{x}$ is created and its probability of been dead is calculated. Figure 8-11 shows the probability field the dead trees population. The big circle is the location of the fieldplot and the small circles are the locations of the dead trees. Please note that the white spots contain no data. Those spots appear either when no LiDAR pulse passes through a column or when the pre-defined height of the shape used to calculate the corresponding feature vector is bigger than the elevation of this point.

8.4.5 Filtering

As shown in Figure Figure 8-11, there is Salt and Pepper noise. This noise is removed using a median filter which assigns to every empty pixel the median value of its non-empty neighbouring pixels (Figure 8-12a). A smoothing filter is further applying for further noise reduction (Figure 8-12b).

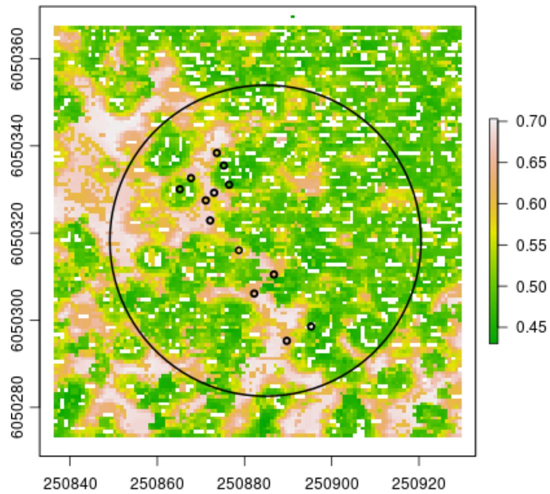

Figure 8-11: The results of the K-NN algorithm

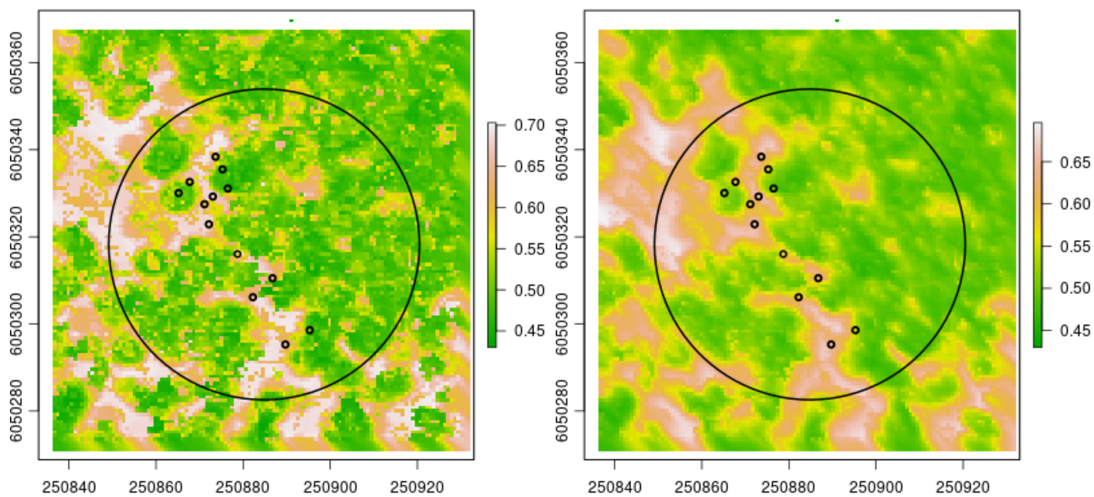

(a) 'Salt and Pepper' noise reduction

(b) Filtering using a smoothing kernel

Figure 8-12: Filtering the results of te K-NN algorithm

8.4.6 Removing Ground Pixels

Removing the ground pixels is a trivial task because the DTM has already subtracted from the data and therefore the height of the ground is approximately constant. A histogram of the height values was generated. As shown in Figure 8-13b, there are three well-defined classes (ground, trees and noise). The ground and noise are removed using two thresholds. This processed is illustrated in Figure 8-13.

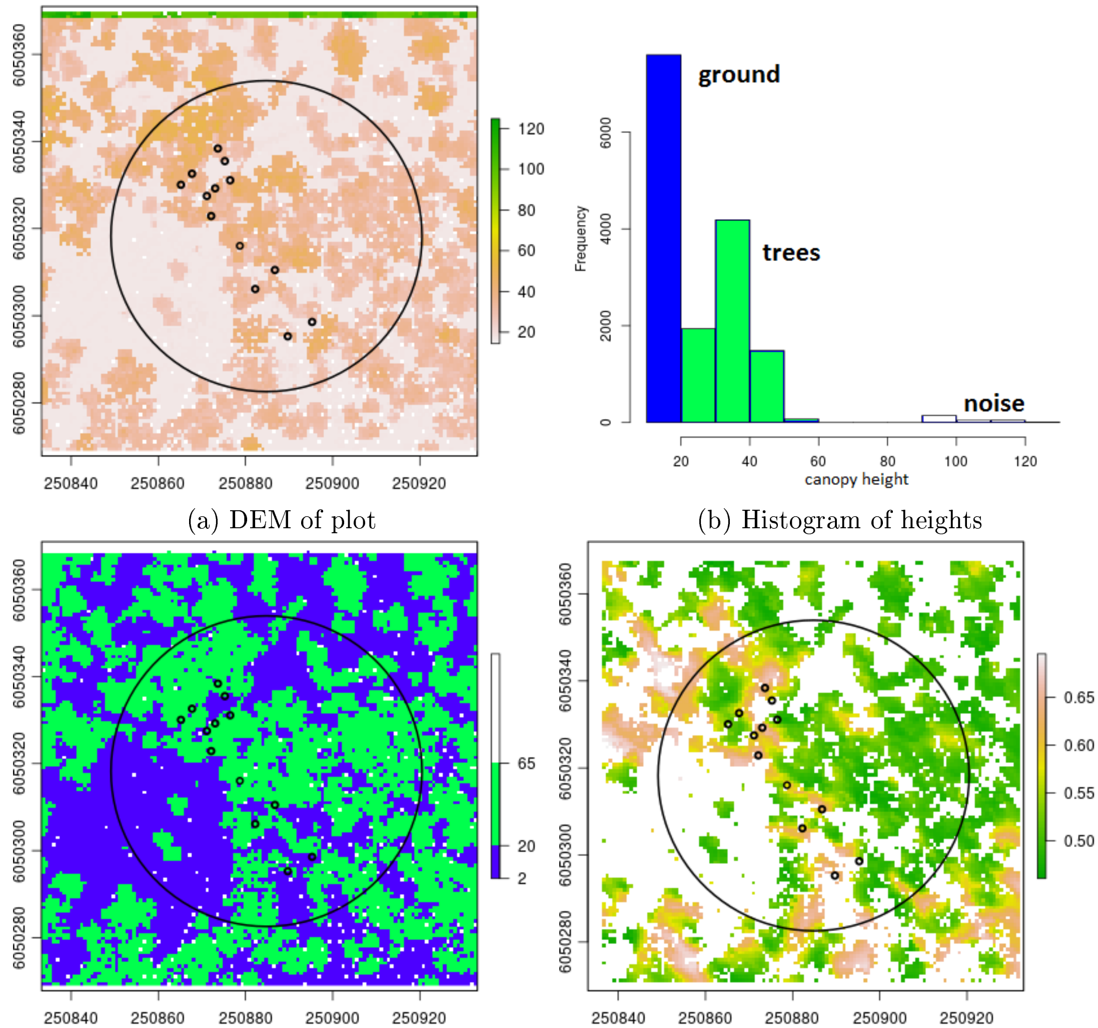

(a) DEM of plot (b) Histogram of heights

(c) Thresholds (d) Results

Figure 8-13: Removing the ground pixels

8.4.7 Dead and Alive Threshold, Filtering, Segmentation and Position Assignment

In order to obtain the estimated positions of the dead trees, there are four steps left:

1. Thresholding
2. Filtering
3. Segmentation
4. Position assignment

Up to this stage, we have an image of the probabilistic field and the ground has been removed (Figure 8-13d). After that a threshold for separating dead and alive pixels is chosen using the training data and the alive pixels are removed (Figure 8-14a). The output image contains out-liners; pixels which are classified as dead but have no neigbouring pixels classified as dead. To reduce over-detection of dead trees, these pixels are filtered out (Figure 8-14b). Afterwards, the pixels are grouped into trees relatively to their neighbouring pixels using a seed growth segmentation algorithm (Algorithm 1 and Figure 8-15a). By the end, it is assumed that each segment S is a dead tree and its position is calculated by taking the average geo-spatial location of the pixels that belong in segment S (Figure 8-15b).

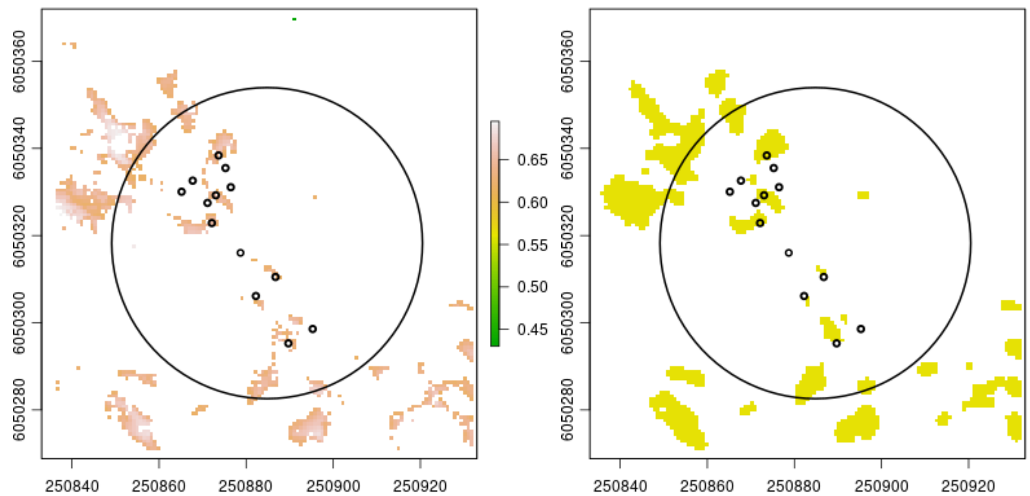

(a) Thresholding dead from alive trees

(b) Noise Reduction

Figure 8-14: Thresholding and filtering

Algorithm 1 Seed growth algorithm for segmenting pixels classified as dead

1: $P \leftarrow$ all pixels classified as dead
2: $s \leftarrow 0$
3: **while** not reached the end of set P **do**
4: get next pixel $\boldsymbol{p} \in P$ that is not assigned to a segment
5: Assign pixel $\boldsymbol{p}$ to segment s
6: find $K(\boldsymbol{p_1}, \ldots, \boldsymbol{p_n})$ such that $K \subseteq P$ and every $\boldsymbol{p_i} \in K$ is a neighbour of $\boldsymbol{p}$
7: $\forall \boldsymbol{p_i} \in K$, $\boldsymbol{p} \leftarrow \boldsymbol{p_i}$ and repeat from line 5
8: all pixels of segment s has been labelled
9: $s \leftarrow s + 1$

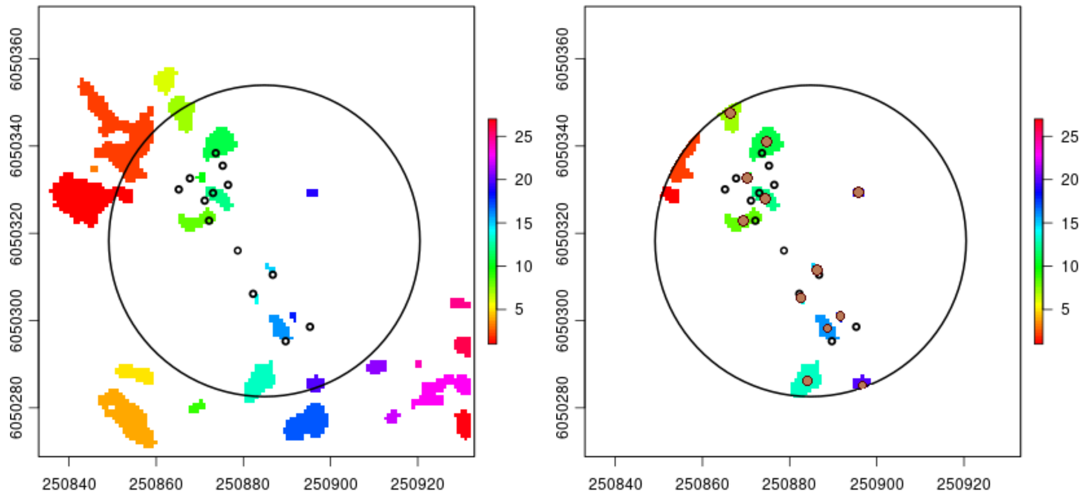

(a) Segmentation using a seed grownth algortihm

(b) The estimated dead tree positions (brown dots)

Figure 8-15: Segmentation and calculating the dead trees' position.

8.5 Evaluation

The results are evaluated according to the predicted locations of the dead trees and their distance from the actual dead trees. There are three different test undertaken during evaluation: whether the increased training samples improves dead tree detection, what shape (cylinder or cuboid) performs better and comparison with a random prediction.

Please note that, the results have been cross-validated using the fieldplots division depicted in Figure 8-9. The 50 field plots are divided into 5 datasets and each dataset uses 10 plots for testing and the rest 40 for evaluation. Additionally, an extra dataset that uses 30 plots for training and 20 for evaluation was created to check whether the increase amount of training samples improves the precision and recall of the results. For each dataset, feature vectors of processed and raw intensities are generated. But Random Forest failed to identify important variable from the feature vectors with the raw intensities due to the irregular shapes of the dead trees. For that reason, results were only obtained from processed voxel intensity values. The feature vectors with raw intensities should be used in other application where trees/object shapes are similar. Additionally, a random set of results was generated for comparison. This random prediction uses the probability of a squared meter to contain a dead tree or not and the number of dead trees assigned to it is approximately the same as the number of dead trees that exist within the field data.

Table 8.4 shows the precission and recall percentage achieved using a cylindrical shape extract features for the likelihood. The D1, D2, ... , D5 corresponds the five divided datasets as they were explained earlier for the cross-validation. The D_1_2_3 uses all the training samples from D1, D2 and D3 to train the classifier. As shown on the corresponding charts (Figure 8-16 for precision and 8-17), the increased amount of training samples do not improve the prediction. On the one hand, more samples contains for dead trees that could be similar to the ones that we want to predict. But on the other hand, as mention in the challenges (Section 8.3, the field data contain noise and therefore the increased noise compensate the value of the increased samples which could have improved the results. A more selective and clean training dataset, that would include trees of similar height and less noise would have definitely improved the results.

Precision (%)										
Distance (m)	1	2	3	4	5	6	7	8	9	10
D1	7.29	12.15	16.1	24.31	32.21	38.9	47.11	49.84	56.23	58.35
D2	2	3.67	8.36	18.39	25.08	33.11	35.78	40.13	46.48	50.5
D3	1.48	5.46	14.2	23.32	29.08	36.6	40.23	46.15	51.38	56.28
D4	0.96	7.24	20.04	28.26	33.09	40.09	44.68	52.17	56.28	62.07
D5	0.75	5.26	8.27	12.03	14.28	21.8	28.57	39.84	47.36	55.63
D_1_2_3	0	8.69	13.04	19.13	24.34	29.56	34.78	36.52	41.73	55.65

Recall (%)										
Distance (m)	2.55	9.26	18.84	32.26	45.04	53.35	56.23	58.78	63.25	68.05
D1	8.22	13.48	23.02	31.25	38.48	51.31	62.17	65.78	66.11	69.07
D2	6.69	14.49	26.55	34.77	40.97	48.6	56.61	59.18	60.71	63.41
D3	5.16	15.5	30.09	38.29	43.46	45.89	51.06	52.58	55.31	57.75
D4	0.89	4.45	12.75	24.03	29.37	35.9	41.83	49.85	59.34	61.12
D5	0	7.22	14.45	20.07	45.19	50.6	51.8	62.65	63.85	73.49
D_1_2_3	0	0	6.17	7.33	8.88	10.03	12.74	20.84	21.62	33.59

Table 8.4: Distance based evaluation: This table gives the percentage of precision and recall achieved using the cylindrical shape to extract features.

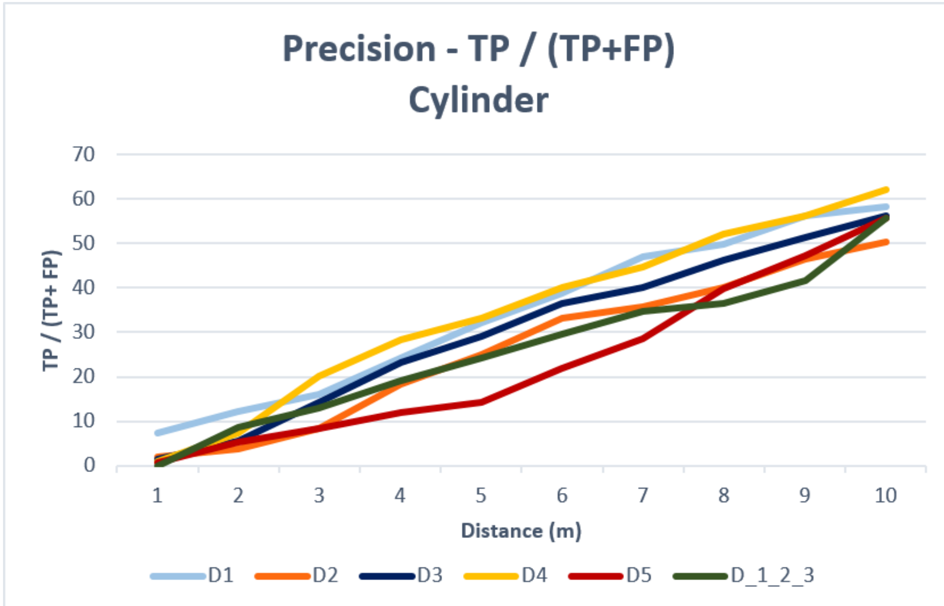

Figure 8-16: Precision results obtained using a cylindrical shape within the voxelised FW LiDAR to extract features. Dataset D_1_2_3 is the dataset that contains more training samples than the rest.

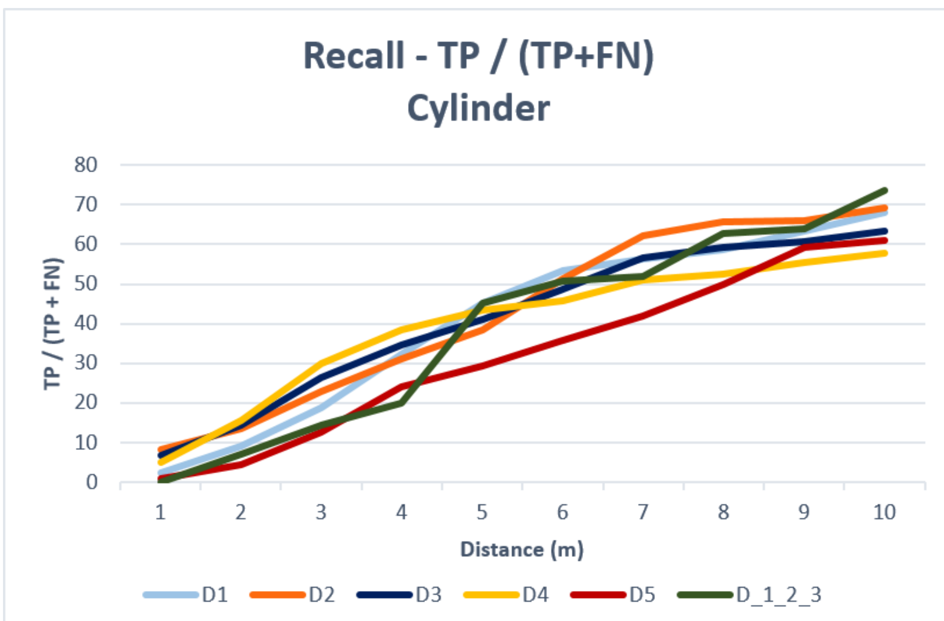

Figure 8-17: Recall results obtained using a cylindrical shape within the voxelised FW LiDAR to extract features. Dataset D_1_2_3 is the dataset that contains more training samples than the rest.

The second comparison is whether a cuboid or a cylindrical shape performs better in extracting useful features for detecting dead tress. The previous Table 8.4 and Figures 8-16 and 8-17 show the results of the prediction using a cylindrical shape to extract features, while Table 8.5 and Figures 8-18 and 8-19 show the results obtained using the cuboid shape. The average results are very close but the cuboid shape has a wider range of good and bad results. It is reasonable for the cylindrical shape to perform better because trees do not have corners and therefore the information retrieved with the cuboid may not be as accurately. Nevertheless, the cuboid shape is slightly bigger and this could be the justification of the wider range of good/bad results. Since it is a bit bigger it may collect better information from big trees but contain more noise in respect to small trees. Therefore, the size of the trees plays a significant role for the quality of the classifier even though in this research we assume equally size trees.

Precision (%)										
Distance (m)	1	2	3	4	5	6	7	8	9	10
D1	7.78	10.47	14.07	24.85	32.63	40.11	47.9	53.59	59.28	61.97
D2	3.66	12.5	16.37	22.84	26.72	34.26	42.02	46.76	51.72	56.68
D3	1.24	3.42	20.56	25.23	29.28	36.76	41.74	43.92	50.15	53.27
D4	8.36	19.86	33.79	36.58	39.02	44.25	50.52	55.05	63.76	66.89
D5	1.96	1.96	5.88	15.68	19.6	25.49	35.29	41.17	45.09	62.74
Recall (%)										
Distance (m)	1	2	3	4	5	6	7	8	9	10
D1	9.58	19.16	35.14	44.4	50.47	56.86	62.93	65.49	69.96	74.76
D2	10.52	20.39	33.22	37.82	47.36	62.17	67.1	70.39	74.01	75.65
D3	5.48	20	31.93	38.7	46.12	54.83	60.64	67.09	72.9	77.09
D4	7.9	17.93	24.92	26.74	33.13	38.29	45.28	47.41	50.75	52.27
D5	4.74	4.74	5.34	11.86	16.02	16.32	21.95	23.73	27.29	31.75

Table 8.5: Distance based evaluation: This table gives the percentage of precision and recall achieved using the Cuboid shape to extract features.

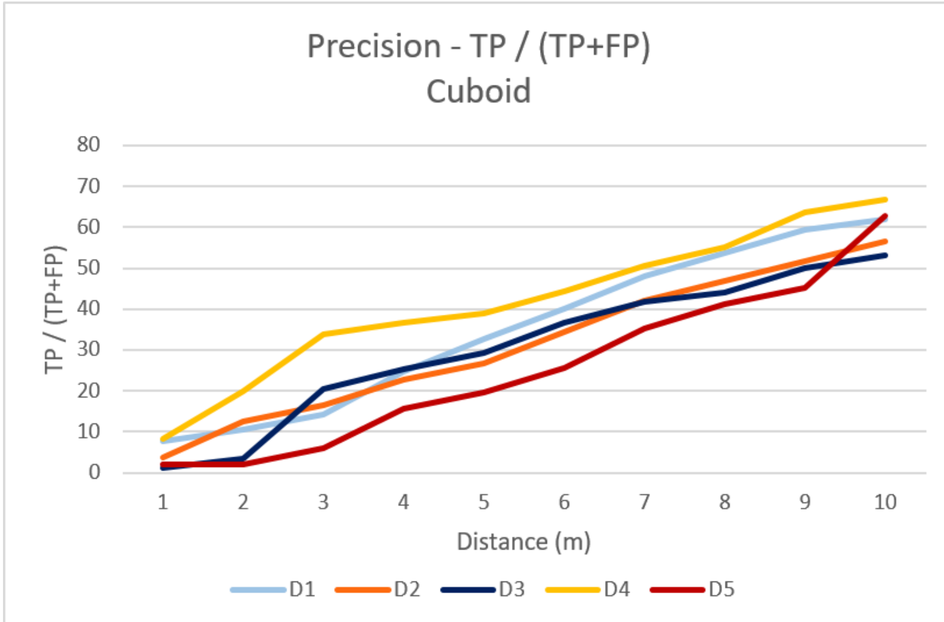

Figure 8-18: Precision results obtained using a cuboid shape within the voxelised FW LiDAR to extract features. Dataset D_1_2_3 is the dataset that contains more training samples than the rest.

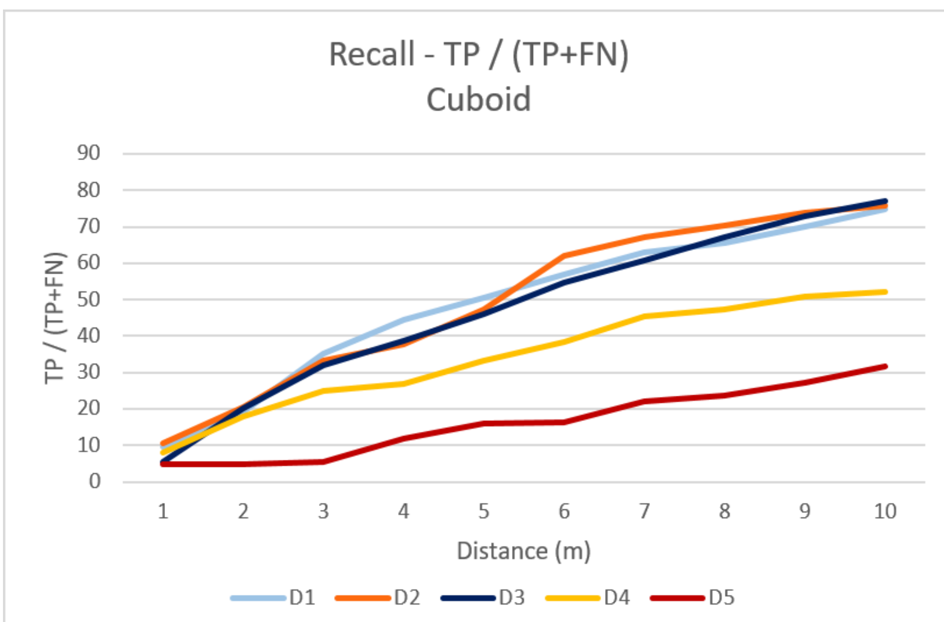

Figure 8-19: Recall results obtained using a cuboid shape within the voxelised FW LiDAR to extract features. Dataset D_1_2_3 is the dataset that contains more training samples than the rest.

The last comparison is in relation to the random. The random dataset distributed randomly within the area of a plot the approximately the same number of dead trees existed. These random location were evaluated the same way as the as the predicted result using the methodology explained in Section 8.4. The average results obtained using a cylindrical shape, a cuboid shape and the random are shown in Table 8.6 and Figures 8-20 and 8-21. Please note that the size of the shapes used is 7.2m diameter or 7.2m width. Therefore, prediction above this distance are above te desire resolution of prediction. From those figures, it is clearly showed that the methodology proposed performs better than the random. This is important because it is an indication that forest health assessment, including dead trees detection, is possible without tree delineation. Of course, the is a new research direction and many improvements could be done; some of them are mentioned after the discussion in the following section.

Precision (%)										
Distance (m)	1	2	3	4	5	6	7	8	9	10
Cylinder	2.50	6.76	13.40	21.27	26.75	34.10	39.28	45.63	51.55	56.57
Cuboid	4.60	9.645	18.14	25.04	29.45	36.18	43.50	48.10	54.00	60.31
Random	0	0	2.56	8.06	11.36	23.81	52.75	57.14	72.16	79.49
Cylinder 1_2_3	0	8.696	13.04	19.13	24.35	29.57	34.78	36.52	41.74	55.65
Recall (%)										
Distance (m)	1	2	3	4	5	6	7	8	9	10
Cylinder	4.71	11.44	22.26	32.13	39.47	47.02	53.58	57.24	60.95	63.88
Cuboid	7.65	16.45	26.11	31.91	38.63	45.70	51.59	54.83	59.00	62.31
Random	0	0	6.18	7.34	8.88	10.04	12.74	20.85	21.62	28.59
Cylinder 1_2_3	0	7.23	14.46	20.07	45.19	50.60	51.81	62.65	63.86	73.49

Table 8.6: Distance based evaluation. This table gives the percentage of precision and recall of the average results of each shape (Cylinder and Cuboid), the Random prediction generated for comparison and the the dataset with that its training dataset is three times larger.

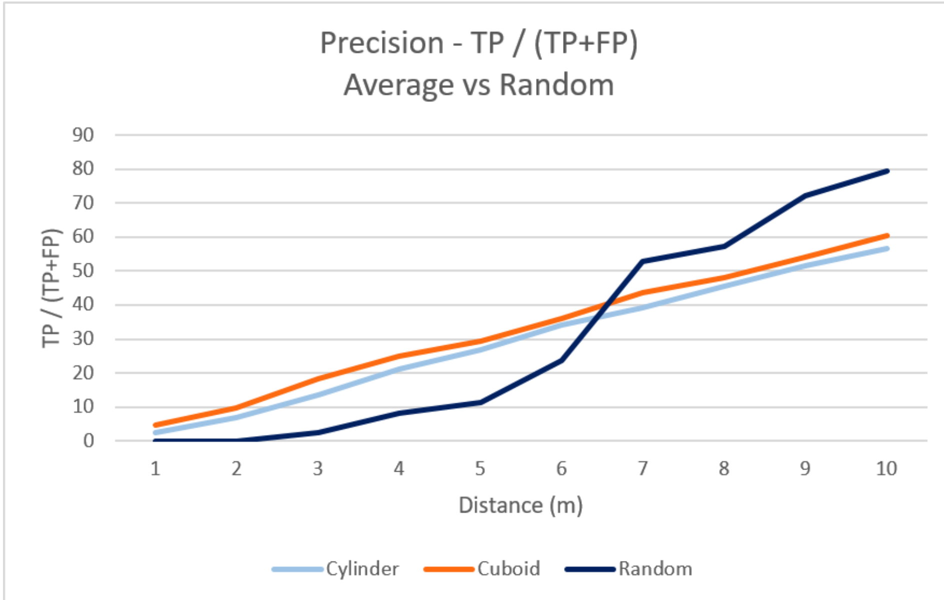

Figure 8-20

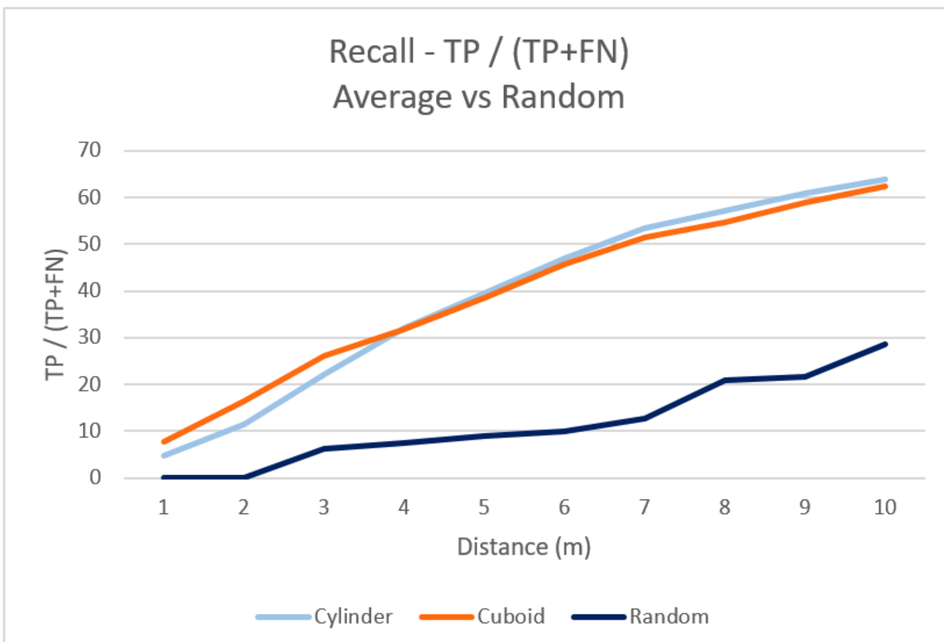

Figure 8-21

8.6 Conclusions and Future Work

The importance of dead wood in forest in large from managing biodiversity. The study area of these project is a native Australian forest with Red River Gum (Eucalyptus) trees, where shortage of hollows for colonisation is predicted and dead trees are more likely to be aged and have hollows.

Previous work on health assesment of forest uses tree delineation but this cannot be applied to eucalyptuses due to their irregular shapes. Additionally the density of the acquired LiDAR data makes bottom to top delineation impossible since information about the trunks are missing. Therefore, this thesis investigates the possibility of detecting dead trees from voxelised FW LiDAR data without tree delineation.

Field data were provided by Forestry Cooperation of NSW, Australia and Interpine Ltd group, New Zealand. The GPS positions of the dead and alive trees within the plots are given but the accuracy is unknown since from the DEM is shown that some trees are not predictable from the data due to their small size.

We use DASOS to extract feature vectors characterising the dead and alive trees and we run them over the volume to generate a 2D image for each testing plot with the probability of a pixel to be a dead tree or not. The ground is afterwards removed and a threshold is defined to separate pixels from dead and alive trees. By the end a seed grown algorithm is used to identify each segment and assign a position for every predicted tree.

Cross validation is used to validate the predicted position of the results. Overall, there are three outcomes. The increase amount of training samples do not improve the results of the classification, probably because while the training datasets becomes bigger the noise increases as well. The feature vectors derived from cylindrical shape are more reliable because the range of the recall and precision percentage was more smaller. By the end, the most important outcome is that the results was clearly better than random prediction, justifying this way that it is possible to identify dead trees without tree delineation.

Nevertheless, this is the first research attempting health forest assesment without tree delineation and this research direction is in early stages and therefore many improvements could be done:

- Manually check and improve position of dead trees using visualisations of the data. In order to improve accuracy of test and evaluating data.
- Separate trees from field data according to their height because tree with different heights have different properties and the size of the objects represented by feature vectors used had constant size.

- Make the size of the object adjustable and derive features that are not height dependant
- Or categorise the trees according to their size and use objects with different sizes.
- After the application of the seed growth algorithm, check the size and shape of the segments and look into the possibility of merging two segments into a single tree or dividing big segments into multiple dead tree prediction.
- The system is usually confused at the edges of the alive trees. Research on how this could be improved. Possibly add negative samples from ground and edges of alive trees.

Chapter 9

Overall Results

Chapter 10

Conclusions

10.1 Contributions

Bibliography

[1] T. Elmqvist, C. Folke, M. Nyström, G. Peterson, J. Bengtsson, B. Walker, and J. Norberg, "Response diversity, ecosystem change, and resilience," *Frontiers in Ecology and the Environment*, vol. 1, no. 9, pp. 488–494, 2003.

[2] D. U. Hooper, F. S. Chapin Iii, J. J. Ewel, A. Hector, P. Inchausti, S. Lavorel, and B. Schmid, "Effects of biodiversity on ecosystem functioning: a consensus of current knowledge," *Ecological monographs*, vol. 75, no. 1, pp. 3–35, 2005.

[3] D. B. Lindenmayer and J. T. Wood, "Long-term patterns in the decay, collapse, and abundance of trees with hollows in the mountain ash (eucalyptus regnans) forests of victoria, southeastern australia," *Canadian Journal of Forest Research*, vol. 40, no. 1, pp. 48–54, 2010.

[4] R. L. Goldingay, "Characteristics of tree hollows used by australian birds and bats," *Wildlife Research*, vol. 36, no. 5, pp. 394–409, 2009.

[5] P. Gibbons and D. Lindenmayer, *Tree Hollows and Wildlife Conservation in Australia*. CSIRO Publishing, 2002.

[6] "Animal pests: Poss." http://www.doc.govt.nz/conservation/threats-and-impacts/animal-pests/animal-pests-a-z/possums/. Accessed: 19th of September 2014.

[7] D. H. DeHayes, P. G. Schaberg, G. J. Hawley, and G. R. Strimbeck, "Acid rain impacts on calcium nutrition and forest health alteration of membrane-associated calcium leads to membrane destabilization and foliar injury in red spruce," *BioScience*, vol. 49, no. 10, pp. 789–800, 1999.

[8] J. Holmgren, "Prediction of tree height, basal area and stem volume in forest stands using airborne laser scanningce," *Scandinavian Journal of Forest Researcht*, vol. 19, no. 6, pp. 543–553, 2004.

[9] S. G. Aracil and R. B. A. Herries, D.L, "Evaluation of an additional lidar metric in forest inventory," *Proceedings of Silvilaser*, 2015.

[10] M. J. Harper, M. A. McCarthy, R. Van Der Ree, and J. C. Fox, "Overcoming bias in ground-based surveys of hollow-bearing trees using double-sampling," *Forest Ecology and Management*, vol. 190, no. 2, pp. 291–300, 2004.

[11] L. Rayner, M. Ellis, and J. E. Taylor, "Double sampling to assess the accuracy of ground-based surveys of tree hollows in eucalypt woodlands," *Forest Ecology and Management*, vol. 36, no. 3, pp. 252–260, 2011.

[12] R. B. Smith, *Introduction to Hyperspectral Imaging.* MicroImages, 2014.

[13] W. Wanger, A. Ullrich, T. Melzer, C. Briese, and K. Kraus, "From single-pulse to ful-waveform airborne laser scanners," *ISPRS Journal of Photogrammetry and Remote Sensing*, vol. 60, pp. 100–112, 2004.

[14] A. Wehr and U. Lohr, "Airborne laser scanning - an introduction and overview," *ISPRS Journal of Photogrammerty and Remote Sensing*, vol. 54, pp. 68–82, 1999.

[15] C. Mallet and F. Bretar, "Full-waveform topographic lidar: State-of-the-art," *ISPRS Journal of Photogrametry and Remote Sensing*, vol. 64, pp. 1–16, 2009.

[16] K. Anderson, S. Hancock, M. Disney, and K. Gaston, "Is waveform worth it? a comparison of lidar approaches for vegetation and landscape characterization," *Remote Sensing in Ecology and Conservation*, 2015.

[17] A. Chauve, C. Mallet, F. Bretar, S. Durrieu, M. Deseilligny, and W. Puech, "Processing full-waveform lidar data: Modelling raw signals," *International Archives of Photogrammetry, Remote Sensing and Spatial Information Sciences*, 2007.

[18] *LAS Specification version 1.3-R1.* Bethesda, Maryland: American Society for Photogrammetry and Remote Sensing, 2010.

[19] M. Warren, *Full Waveform Upgrade.* NERC ARSF wiki, 2012.

[20] M. J. Sumnall, R. A. Hill, and S. A. Hinsley, "Comparison of small-footprint discrete return and full waveform airborne lidar data for estimating multiple forest variables," *Remote Sensing of Environment*, vol. 173, pp. 214–223, 2016.

[21] K. H. R. A. . Z. A. Lehner, H., "Consideration of laser pulse fluctuations and automatic gain control in radiometric calibration of airborne laser scanning data.," *Proceedings of 6th ISPRS Student Consortium and WG VI/5 Summer School*, 2011.

[22] I. Korpela, H. O. Ørka, H. V. Hyyppä, J., and T. Tokola, "Range and agc normalization in airborne discrete-return lidar intensity data for forest canopies," vol. 65, no. 4, pp. 369–379, 2010.

[23] M. Isenburg, *LAStools - efficient tools for LiDAR processing*. rapidlasso.

[24] M. Warren, B. Taylor, M. Grant, and J. D. Shutler, "Data processing of remorely sensed airborne hyperspectral data using the airborne processing library (apl)," *ScienceDirect, Computers and Geosciences*, vol. 64, 2014.

[25] M. Isenburg, "Pulsewaves: An open, vendor-neutral, stand-alone, las-compatible full waveform lidar standard.," 2012.

[26] A. Persson, U. Soderman, J. Topel, and S. Ahlberg, *Visualisation and Analysis of full-waveform airborne laser scanner data*. V/3 Workshop, Laser scanning 2005, 2005.

[27] M. Miltiadou, M. A. Warren, M. Grant, and M. Brown, "Alignment of hyperspectral imagery and full-waveform lidar data for visualisation and classification purposes," *The International Archives of Photogrammetry, Remote Sensing and Spatial Information Sciences*, vol. 40, no. 7, p. 1257, 2015.

[28] W. Wanger, A. Ullrich, V. Ducic, T. Maizer, and N. Studnicka, "Gaussian decompositions and calibration of a novel small-footprint full-waveform digitising airborne laser scanner," *ISPRS Journal of Photogrammetry and Remote Sensing*, vol. 60, pp. 100–112, 2006.

[29] A. Neuenschwander, L. Magruder, and M. Tyler, "Landcover classification of small-footprint full-waveform lidar data," *Jounal of Applied Remote Sensing*, vol. 3, no. 1, pp. 033544–033544.

[30] J. Reitberger, P. Krzystek, and U. Stilla, "Analysis of full waveform LiDAR data for tree species classification," *International Journal of Remote Sensing*, vol. 29, no. 5, pp. 1407–1431, 2008.

[31] A. Chauve, F. Bretar, S. Durrieu, M. Pierrot-Deseilligny, and W. Puech, "Fullanalyze: A research tool for handling, processing and analysing full-waveform lidar data," *IEEE International Geoscience and Remote Sensing Symposium*, 2009.

[32] P. Bunting, J. Armston, D. Clewley, and R. M. Lucas, "Sorted pulse data (spd) library—part ii: A processing framework for lidar data from pulsed laser systems in terrestrial environments," *Computers & Geosciences*, vol. 56, pp. 207–215, 2013.

[33] L. Cao, N. Coops, L. Innes, J. Dai, and H. Ruan, "Tree species classification in subtropical forests using small-footprint full-waveform lidar data," *International Journal of Applied Earth Observation and Geoinformation*, vol. 49, pp. 39–51, 2016.

[34] S. Hancock, K. Anderson, M. Disney, and K. J. Gaston, "Measurement of fine-spatial-resolution 3d vegetation structure with airborne waveform lidar: Calibration and validation with voxelised terrestrial lidar.," *Remote Sensing of Environment*, vol. 188, pp. 37–50, 2017.

[35] M. Miltiadou, M. Grant, M. Brown, M. Warren, and E. Carolan, "Reconstruction of a 3d polygon representation from full-wavefrom lidar data," *RSPSoc Annual Conference 2014, New Sensors for a Changing World*, 2014.

[36] R. Crippen, "Calculating the vegetation index faster," *Remote Sensing of Environment*, vol. 34, no. 1, pp. 71–73, 1990.

[37] R. N. Clark, G. A. Swayze, R. Wise, K. E. Livo, T. Hoefen, R. F. Kokaly, and S. J. Sutley, "Usgs digital spectral library splib06a," *US Geological Survey, Digital Data Series*, vol. 231, 2007.

[38] P. Hanrahan, "Ray tracing algebraic surfaces," *ACM SIGGRAPH Computer Graphics*, vol. 17, no. 3., 1983.

[39] H. Pfister, J. Hardenbergh, J. Knittel, H. Lauer, and L. Seiler, "The volumepro real-time ray-casting system," *Proceedings of the 26th annual conference on Computer graphics and interactive techniques*, pp. 251–260, 1999.

[40] J. Nickolls, I. Buck, M. Garland, and K. Skadron, "Scalable parallel programming with cuda," *Queue*, vol. 6, no. 2, pp. 40–55, 2008.

[41] C. Crassin, F. Neyret, S. Lefebvre, and E. Eisemann, "Gigavoxels: Ray-guided streaming for efficient and detailed voxel rendering," *Proceedings of the 2009 symosium on Interactive 3D graphics and games*, pp. 15–22, 2009.

[42] J. F. Blinn, *A Generalization of Algebraic Surface Drawing*, vol. 1. ACM Transactions on Graphics (TOG).

[43] A. Pasko and V. Savchenko, *Blending operations for the functionally based constructive geometry.* 1994.

[44] W. E. Lorensen and H. E. Cline, "Marching cubes: A high resolution 3d surface construction algorithm," *ACM Siggraph Computer Graphics*, vol. 21, pp. 163–169, 1987.

[45] M. Levoy, "Volume rendering: Display of surfaces from volume data," *IEEE Computer Graphics and Applications*, vol. 8, no. 3, pp. 29–37, 1998.

[46] M. Hadwiger, J. Beyer, W. K. Jeong, and H. Pfister, "Interactive volume exploration of patascale microscopy data streams using visualizatin-driven virtual memory approach," *IEEE Transactions on Visualisation and Computer Graphics*, 2012.

[47] S. Laine and T. Karras, "Efficient sparse voxel octrees," *Visualization and Computer Graphics, IEEE Transactions*, vol. 17, no. 8, pp. 1048–1059, 2011.

[48] B. Rodrigues de Araujo and J. A. Pires Jorge, *Adaptive polygonization of implicit surfaces*, vol. 29. Science Direct, Computer and Graphics, 2005.

[49] E. Hartmann, "A marching method for the triangulation of surfaces," *The Visual computer 14, no*, vol. 14, no. 3, pp. 95–108, 1998.

[50] C. D. Hansen and P. Hinker, "Massively parallel isosurface extraction," *Proceedings of the 3rd conference on Visualization '92*, pp. 77–83, 1992.

[51] C. Galbraith, P. MacMurchy, and B. Wyvill, *BlobTree Trees.* IEEE Computer Graphics International, 2004.

[52] H. Sutter and A. Alexandrescu, *C++ Coding Standards: 101 Rules, Guidlines, and Best Practices.* United States: Addison-Wesley, 2004.

[53] J. Wilhelms and A. Van Gelder, "Octrees for faster isosurface generation," vol. 24, no. 5, 1990.

[54] . W. J. Schaefer, S., "Dual marching cubes: Primal contouring of dual grids," *Computer Graphics Forum*, vol. 24, no. 2, 2005.

[55] J. Wilhelms and A. Van Gelder, "Octrees for faster isosurface generation," *ACM Transactions on Graphics (TOG)*, vol. 11, no. 3, pp. 201–227, 1992.

[56] S. F. Gibson, "Constrained elastic surface nets: Generating smooth surfaces from binary segmented data," *International Conference on Medical Image Computing and Computer-Assisted Intervention*, pp. 888–898, 1998.

[57] B. Chazelle and L. J. Guibas, "Fractional cascading: I. a data structuring technique.," *Algorithmica.*

[58] K. Museth, “Vdb: High-resolution sparse volumes with synamic topology,” *ACM Transactions on Graphics (TOG)*, vol. 32, no. 3, p. 27, 2013.

[59] M. S. Warren and J. K. Salmon, “A parallel hashed oct-tree n-body algorithm,” *In Proceedings of the 1993 ACM/IEEE conference on Supercomputing*, pp. 12–21, 1993.

[60] M. Nießner, M. Zollhöfer, S. Izadi, and M. Stamminger, “Real-time 3d reconstruction at scale using voxel hashing,” *ACM Transactions on Graphics (TOG)*, vol. 32, no. 2, p. 169, 2013.

[61] F. C. Crow, “Summed-area tables for texture mapping,” *ACM Computer Graphics*, vol. 18, no. 3, pp. 207–212, 1984.

[62] S. Hanan, “Neighbor finding in images represented by octrees,” *Computer Vision, Graphics, and Image Processing*, vol. 46, no. 3, pp. 367–386, 1989.

[63] G. Schrack, “Finding neighbors of equal size linear quadtrees and octrees in constant time,” *CVGIP: Image Understanding*, vol. 55, no. 3, pp. 221–230, 1992.

[64] R. Lohner, “Robust, vectorized search algorithms for interpolation on unstructured grids,” *Journal of Computational Physics*, vol. 118, no. 2, pp. 380–387, 1995.

[65] R. Castro, T. Lewiner, H. Lopes, G. Tavares, and A. Bordignon, “Statistical optimisation of octree searches,” *Computer Graphics Forum*, vol. 27, no. 6, pp. 1557–1566, 2008.

[66] M. L. Clark, D. A. Roberts, J. J. Ewel, and D. B. Clark, “Estimation of tropical rain forest aboveground biomas with small-foorprint lidar and hyperspectral sensors,” *ScienceDirect, Remote Sensing of Enviroment*, vol. 115.

[67] J. E. Anderson, L. C. Plourde, M. E. Martin, B. H. Braswell, M. L. Smith, R. O. Dubayah, M. A. H. Dubayah, and J. B. Blair, “Integrating waveform lidar with hyperspectral imagery for inventory of a northern temperate forest,” *Remote Sensing of Environment*, vol. 112, no. 4, pp. 1856–1870, 2008.

[68] H. Buddenbaum, S. Seeling, and J. Hill, “Fusion of full-waveform lidar and imaging spectroscopy remote sensing data for the characterization of forest stands,” *International Journal of Remote Sensing*, vol. 32, no. 13, pp. 4511–4524, 2013.

[69] J. Heinzel and B. Koch, “Investigating multiple data sources for tree species classification in temperate forest and use for single tree delineation,” *International*

Journal of Applied Earth Observation and Geoinformation, vol. 18, pp. 101–110, 2012.

[70] R. G. Congalton, "A review of assessing the accuracy of classifications of remotely sensed data," *Remote Sensing of Enviroment*, vol. 37, no. 1.

[71] J. F. Franklin, H. H. Shugart, and M. E. Harmon, "Tree death as an ecological process," *BioScience*, vol. 17, no. 8, pp. 550–556, 1987.

[72] J. Siitonen, "Forest management, coarse woody debris and saproxylic organisms: Fennoscandian boreal forests as an example," *Ecological bulletins*, pp. 11–41, 2001.

[73] I. Hanski, "Extinction debt and species credit in boreal forests: modelling the consequences of different approaches to biodiversity conservation," *Annales Zoologici Fennici*, pp. 271–280, 2000.

[74] G. Peterson, C. R. Allen, and C. S. Holling, "Ecological resilience, biodiversity, and scale.," *Ecosystems*, vol. 1, no. 1, pp. 6–18, 1998.

[75] N. Abrego and I. Salcedo, "How does fungal diversity change based on woody debris type? a case study in northern spain," *Ekologija*, vol. 57, no. 3, 2011.

[76] J. N. Stokland and K. H. Larsson, "Legacies from natural forest dynamics: Different effects of forest management on wood-inhabiting fungi in pine and spruce forests," *Forest Ecology and Management*, vol. 261, no. 11, pp. 1707–1721, 2011.

[77] D. Lonsdale, M. Pautasso, and O. Holdenrieder, "Wood-decaying fungi in the forest: conservation needs and management options," *European Journal of Forest Research*, vol. 127, no. 1, pp. 1–22, 2008.

[78] "List of extinct, threatened and near threatened australian birds," *Environment Protection and Biodiversity Conservation Act*, 1999.

[79] Government of Western Australia, "Oarks and wildlife the list of threatened and priority fauna list," tech. rep., November 2015.

[80] Y. Kim, Z. Yang, W. B. Cohen, D. Pflugmacher, C. L. Lauver, and J. L. Vankat, "Distinguishing between live and dead standing tree biomass on the north rim of grand canyon national park, usa using small-footprint lidar data.," *Remote Sensing of Environment*, vol. 113, no. 11, pp. 2499–2510, 2009.

[81] P. Polewski, W. Yao, M. Heurich, P. Krzystek, and U. Stilla, "Detection of fallen trees in als point clouds using a normalized cut approach trained by simulation,"

ISPRS Journal of Photogrammetry and Remote Sensing, vol. 105, pp. 252–271, 2015.

[82] W. Mücke, B. Deák, H. M. Schroiff, A., and N. Pfeifer, "Detection of fallen trees in forested areas using small footprint airborne laser scanning data," *Canadian Journal of Remote Sensing*, vol. 139, no. s1, pp. S32–S40, 2013.

[83] W. Yao, P. Krzystek, and M. Heurich, "Identifying standing dead trees in forest areas based on 3d single tree detection from full-waveform lidar data," *ISPRS Annals of the Photogrammetry, Remote Sensing and Spatial Information Sciences*, vol. I-7, pp. 359–364, 2012.

[84] J. Pasher and D. J. King, "Mapping dead wood distribution in a temperate hardwood forest using high resolution airborne imagery," *Forest Ecology and Management*, vol. 258, no. 7, pp. 1536–1548, 2009.

[85] I. Shendryk, M. Broich, M. G. Tulbure, A. McGrath, D. Keith, and S. V. Alexandrov, "Mapping individual tree health using full-waveform airborne laser scans and imaging spectroscopy: A case study for a floodplain eucalypt forest," *Remote Sensing of Environment*, vol. 187, pp. 202–217, 2016.

[86] S. C. Popescu, R. H. Wynne, and R. F. Nelson, "Measuring individual tree crown diameter with lidar and assessing its influence on estimating forest volume and biomass," *Canadian journal of remote sensing*, vol. 29, no. 5, pp. 564–577, 2003.

[87] L. Jing, B. Hu, J. Li, and T. Noland, "Automated delineation of individual tree crowns from lidar data by multi-scale analysis and segmentation," *Photogrammetric Engineering & Remote Sensing*, vol. 78, no. 12, pp. 1275–1284, 2012.

[88] B. Hu, J. Li, L. Jing, and A. Judah, "Improving the efficiency and accuracy of individual tree crown delineation from high-density lidar data," *International Journal of Applied Earth Observation and Geoinformation*, vol. 26, pp. 145–15, 2014.

[89] S. C. Popescu and K. Zhao, "A voxel-based lidar method for estimating crown base height for deciduous and pine trees," *Remote sensing of environment*, vol. 112, no. 3, pp. 767–781, 2008.

[90] I. Shendryk, M. Broich, M. G. Tulbure, and S. V. Alexandrov, "Bottom-up delineation of individual trees from full-waveform airborne laser scans in a structurally complex eucalypt forest," *Remote Sensing of Environment*, vol. 173, pp. 69–83, 2016.

[91] J. L. Lovell, D. L. B. Jupp, G. J. Newnham, N. C. Coops, and D. S. Culvenor, "Simulation study for finding optimal lidar acquisition parameters for forest height retrieval.," *Forest Ecology and Management*, vol. 214, no. 1.

[92] P. Viola and M. Jones, "Rapid object detection using a boosted cascade of simple features," *Computer Vision and Pattern Recognition*, vol. 1, 2001.

[93] P. Dong, "Characterization of individual tree crowns using three-dimensional space signatures derived from lidar data.," *International Journal of Remote Sensing*, vol. 30, no. 24, pp. 6621–6628, 2009.

[94] J. Kerle, "Collation and review of stem density data and thinning prescriptions for the vegetation communities of new south wales," 2005.

[95] N. Wilson and N. C. C. of N.S.W, "The flooded gum trees : land use and management of river red gums in new south wales," *The Council, Sydney*, 1995.

[96] E. van Rees, "Trimble's ax60i and ax80," *GeoInformatics*, vol. 7, no. 5.

[97] M. Miltiadou, N. D. F. Campbell, M. Brown, A. S. G., M. Warren, D. Clewley, and M. Grant, "User guide of the 2nd version o dasos," 2017.

[98] A. Liaw and M. Wiener, "Classification and regression by randomforest," *R news*, vol. 2, no. 3.

[99] M. Sumnall, *Assessment of habitat condition and conservation status for lowland British woodland using earth observation techniques.* Bournemouth University: Unpublished PhD thesis, 2013.

Appendices

Appendix A

DASOS's user guide, released on the 20th of January 2017

Appendix B

Case Study: Field Work in New Forest